IEEE Transactions on Quantum Engineering

Received 3 July 2025; accepted 17 September 2025; date of publication 1 October 2025; date of current version 5 November 2025.

Digital Object Identifier 10.1109/TQE.2025.3616080

Quasiparticle Dynamics in Niobium Nitride Superconducting Microwave Resonators at Single-Photon Regime

PANIZ FOSHAT[1], SHIMA POORGHOLAM-KHANJARI[1], VALENTINO SEFERAI[1], HUA FENG[1], SUSAN JOHNY[1], OLEG A. MUKHANOV[2], MATTHEW HUTCHINGS[3], ROBERT H. HADFIELD[1], MARTIN WEIDES[1], AND KAVEH DELFANAZARI[1]

[1]Electronics and Nanoscale Engineering Division, James Watt School of Engineering, University of Glasgow, G12 8QQ Glasgow, U.K.
[2]SEEQC, Elmsford, NY 10523 USA
[3]SEEQC, SE1 9PG London, U.K.

Corresponding author: Kaveh Delfanazari (e-mail: kaveh.delfanazari@glasgow.ac.uk).

This work was supported in part by the Royal Academy of Engineering under Grant LTRF2223-19-138, in part by the Royal Society of Edinburgh under Grant 319941, and in part by Royal Society under Grant RGS222168, Grant EPSRC PRF-11-I-08, and Grant EPSRC EP/X025152/1.

ABSTRACT Reliable operation of superconducting quantum circuits demands effective control over quasiparticles, which introduce energy distributions below the superconducting gap and act as a dominant source of decoherence. Here, we investigate the impact of quasiparticle dynamics on niobium nitride (NbN) microwave coplanar waveguide resonators on silicon chips. By performing sub-Kelvin measurements of resonance frequency and internal quality factor across temperature sweeps, we find links between quasiparticle energy and superconducting circuit performance. Calculations of the complex conductivity of the NbN film reveal the quantitative role of quasiparticle density in experimental results. These findings deepen understanding of quasiparticle-induced losses, paving the way toward engineering more resilient superconducting resonators, with broad implications for scalable and fault-tolerant quantum computing architectures.

INDEX TERMS Circuit quantum electrodynamics (cQED), quantum computing, quasiparticle loss, single-photon superconducting microwave circuits, superconducting microwave coplanar waveguide resonators (CPW).

I. INTRODUCTION

Boosting coherence time has become crucial for maximizing the efficiency of superconducting quantum circuits [1], especially in Cooper pair transistors [2], kinetic inductance detectors [3], [4], [5], and superconducting qubits [6].

The presence of charge carriers that participate in superconducting condensate, known as quasiparticle poisoning [7], is currently one of the primary reasons limiting the performance of superconducting quantum circuits [8], [9], [10], [11]. Moreover, recent studies indicate that in multiqubit systems, quasiparticle emergence can suppress the qubit relaxation time since quasiparticles are coupled with all qubits in a wafer-scale chip [12]. Research demonstrates that quasiparticles' impact on the performance of quantum circuits can be reduced or eliminated by carefully selecting materials [13] and engineering designs [14], [15], [16]. For example, including quasiparticle' traps made of a lower gap superconductor on the quantum circuit is effective for this purpose [17]. Therefore, characterizing the quasiparticle dynamics of superconductor films is important in the development of superconducting qubits and quantum circuits [12], [18].

Niobium nitride (NbN) is a type II superconductor with promising applications in unconventional superconducting quantum circuits [19]. Recent studies have shown that superconductors–semiconductor nanodevices can host Majorana quasiparticles or be utilized in Andreev-based superconducting circuits [20], [21]. Given that NbN can operate in quantum circuits at higher temperatures, wider frequencies, and under higher magnetic fields, it is essential to investigate the behavior and presence of quasiparticles across different temperatures. To do so, we fabricate NbN superconducting microwave coplanar waveguide (CPW) resonators, as they are fundamental elements in most quantum circuits.

For this study, we selected a 100 nm thickness (t) NbN film as a tradeoff between low-loss characteristics and robustness

against magnetic fields of the superconducting film. While thicker films are typically used in transmon qubits, they are often more susceptible to the extensive magnetic field effects on CPWs' properties, such as resonance frequency (f_r) and internal quality factor (Q_i), due to the emergence of Abrikosov vortices. Our previous work demonstrated that 100 nm NbN films provide a high Q_i with and without the presence of the magnetic field [22], making them a suitable choice for investigating quasiparticle dynamics in hybrid superconductor–semiconductor circuits. Moreover, CPWs are a powerful and valuable tool for measuring the losses of superconducting films [23]. CPW resonators characterize losses, such as two-level system (TLS) defects [24], nonequilibrium quasiparticles [25], [26], [27], vortices [28], [29], and microwave radiation [30], [31], in superconducting circuits. Calculating and modeling TLS defects is relatively straightforward in superconducting CPW; however, resolving quasiparticle losses requires intensive computational calculations. Theoretical predictions indicate that Cooper pair breaking should be negligible at temperatures much lower than the critical temperature (T_c) due to insufficient thermal energy to break the pairs. However, experimental results in materials, such as aluminum (Al) [32], [33] and titanium nitride (TiN) [34], show a persistent presence of quasiparticles even at temperatures significantly below T_c. While limited research has been done on quasiparticle density in Nb-based superconducting films [35], [36], there is a significant gap in the research on quasiparticle density focusing on Nb-based CPW.

Here, we will have a more in-depth discussion on characterizing quasiparticles' emergence in superconducting microwave CPW resonators. We model TLS loss with a standard conventional model [22], [24], [37]. To describe quasiparticle loss, we calculate the complex conductivity of the NbN film based on Mattis–Bardeen theory [38], [39].

On the measurement side, we conduct a dc measurement of the NbN film to find T_c and resistivity in the normal state ($R_\square$). Moreover, we perform cryogenic microwave spectroscopy of the NbN superconducting CPW resonators to find the effect of temperature sweep $T < \frac{T_c}{3}$ on the measured Q_i and resonance frequency shift (Δf). We successfully maintain a high $Q_i > 7 \times 10^3$ at temperatures below 3 K. We prove the reliability of the Q_i measurements by comparing the measurement results with analytical calculations.

II. FABRICATION METHOD

In our design, three resonators are capacitively coupled to a common feedline, with 4 μm width and 2 μm gap.

To fabricate the superconducting circuit, we dipped a high-resistivity silicon wafer into buffer oxide etchant to strip the SiO_x layer and prepare it for superconducting film deposition. Immediately after, the wafer was placed in a sputtering system to form a 100 nm NbN film. The NbN film was formed through reactive dc sputtering using an argon (Ar) and nitrogen (N_2) plasma [40]. Table 1 illustrates the details of the sputtering process of the NbN film. Two samples of the chip were used after dicing: one to pattern the resonators with standard e-beam lithography, followed by CF_4 anisotropic dry etch, and the other was used for dc measurement.

TABLE 1. NbN Film Sputtering Process Information

Ar	N_2	Base current	Sputtering time
25 sccm	3 sccm	0.85 A	15 min

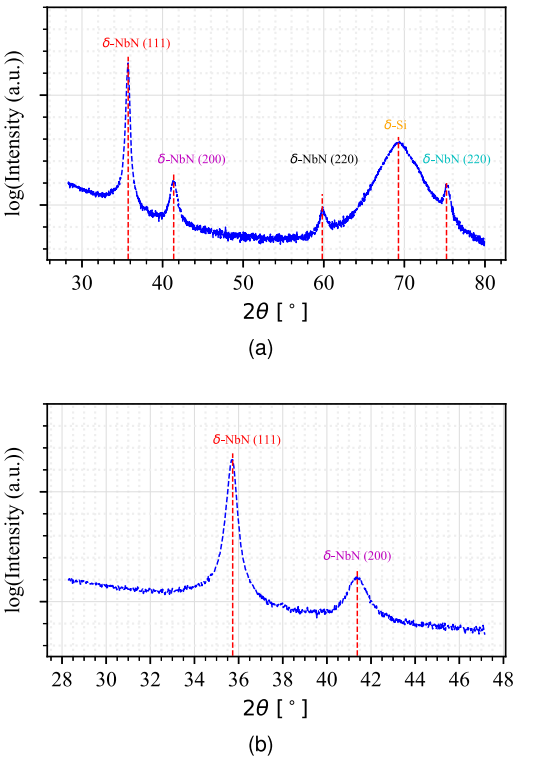

FIG. 1. (a) XRD pattern of the NbN film. (b) Zoomed-in region (30°–48°) showing diffraction peaks associated with the superconducting phases of NbN.

It should be noted that silicon was selected as the substrate in our CPWs chips because of its compatibility with the fabrication process of advanced semiconductor devices and hybrid superconductor–semiconductor circuits. Although other substrates, such as sapphire, offer advantages in terms of reduced dielectric loss, silicon remains the preferred choice because of its compatibility with industrial semiconductor fabrication processes. However, coherence times in these types of hybrid quantum circuit remain a key limitation to further scaling them. Addressing this challenge requires comprehensive research, and we have taken the initial step toward it in this article. As for the superconducting material, we concentrated on depositing NbN films to achieve low-loss superconducting films that are well suited for the simple fabrication of robust hybrid superconductor–semiconductor circuits, such as through room temperature deposition of the NbN film.

To further investigate the structure and composition of our NbN film, we examined our sample with X-ray diffractometry to determine its orientation and phase purity. Fig. 1(a) displays the X-ray diffraction (XRD) pattern of our NbN film. In Fig. 1(b), we observed the prominent peaks corresponding to the (111) and (200) oriented grains of cubic

IEEE Transactions on Quantum Engineering

TABLE 2. XRD Pattern Data Including: Orientation, Peak Position, FWHM, Grain Size, and Lattice Size of NbN Film

Orientation	2θ (^{o})	FWHM (^{o})	Grain Size (nm)	a (Å)
(111)	35.73	0.47	176.07	4.35
(200)	41.38	1.36	62.54	4.36
(022)	59.81	1.67	54.89	4.37
(222)	75.23	1.44	69.57	4.37

δ-NbN film at 35.7° and 41.3°, respectively. We also noticed two further peaks at 59.8° and 75.2°, which can be assigned to the grains of (022) and (222) orientation of NbN film [41], [42], [43]. The full-width at half maximum (FWHM) of the (111) and (200) peaks were measured to be 0.47° and 1.36°, respectively. The sharper (111) peak is useful, as it is often associated with improved electrical and superconducting properties in δ-NbN films [41]. Peak broadening, as observed in the (200), (022), and (222) reflections, may be attributed to reduced crystallite size, microstrain, or structural defects. The calculated lattice constant (a) from the (111), (200), (022), and (222) peaks ranges from 4.35 to 4.37 Å, lower than the ideal δ-NbN value of $a = 4.45$ Å. This slight difference indicates a nonideal lattice possibly due to strain, mechanical stress, and induced defects in NbN film [44], [45]. Table 2 summarizes the above information.

III. DC MEASUREMENT

We characterized the NbN film by performing cryogenic dc transport measurements of a 15 mm × 15 mm chip between the temperature ranges from 2 K to room temperature to find the film parameters, such as T_c, sheet resistance $R_\square(T_c)$, and residual resistive ratio (RRR). Fig. 2(a) shows the schematic illustration of the wafer and the detail of the diced silicon wafer after dicing (bottom) used for dc measurements. Fig. 2(b) illustrates the extracted $T_c = 10.7 \pm 0.5$ K and $R_\square(T_c) = 159.5\ \Omega$, respectively. Although achieving NbN films with higher T_c is possible [46], [47], through varying deposition parameters, such as substrate heating, the room temperature magnetron sputtering employed in this study was selected to ensure compatibility with the fabrication process of hybrid superconductor–semiconductor quantum circuits. However, this process remains open to further optimization, such as by modifying sputtering parameters and applying postdeposition treatments, to improve superconducting T_c while preserving compatibility with the superconductor–semiconductor fabrication process. We note that the T_c reported here is not the upper limit; higher values ($T_c \approx 12.05$ K) were later obtained on different substrates with improved sputtering tool conditions, although these results are beyond the scope of this work.

IV. TEMPERATURE-DEPENDENT MICROWAVE SPECTROSCOPY OF CPW RESONATORS

Theoretically, any phonon or photon with energy greater than the superconducting energy gap (2Δ) can break Cooper pairs and generate quasiparticles. These quasiparticles will create resistive and inductive channels in the CPW resonators [48]. Emerging new inductive and resistive channels based

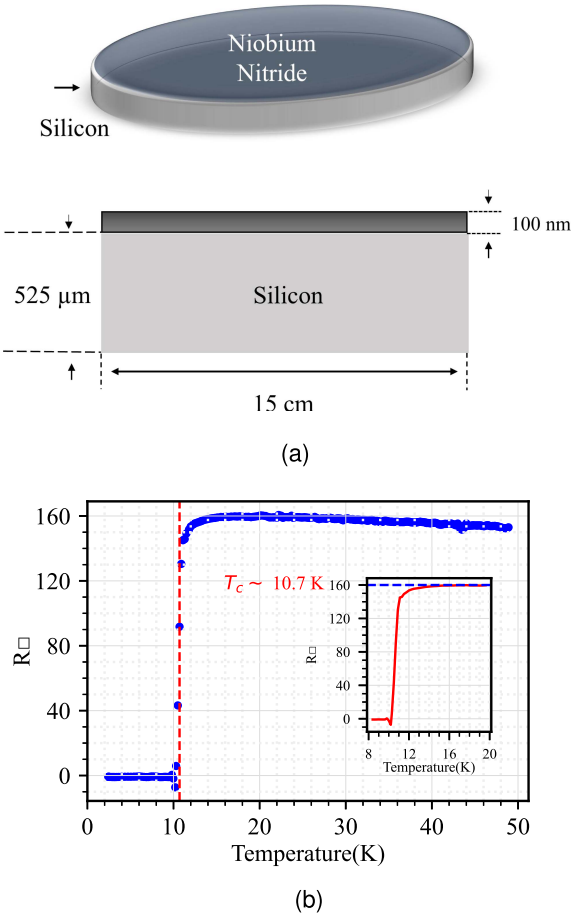

FIG. 2. (a) Top view and cross section illustrations of a 100nm NbN thin film sputtered on a 525-μm-thick silicon wafer for cryogenic dc transport and RF spectroscopy measurements. (b) Sheet resistance versus temperature for the NbN/silicon chip. RRR is estimated to be $R_{300K}/R_{T_c} \approx 0.98$.

on quasiparticle density in CPW will affect its propagation properties. Calculating the superconducting resonator's surface impedance will help predict and confirm f_r and Q_i as a function of quasiparticle density. The surface impedance of the superconductor depends on the film thickness, d, mean free path, l, coherence length, ξ, and penetration length, λ. In the superconducting dirty limit condition, where $l \ll \xi$ and $l \ll \lambda$, surface impedance and quasiparticle loss can be written as [48], [49]:

$$Z_s(T) = \sqrt{\frac{j\mu_0\omega}{\sigma_1(T) - j\sigma_2(T)}} = R_s + j\omega L_s \quad (1)$$

$$\delta_{\text{qp,Theory}}(T) \sim \frac{\text{Re}(Z_s(T))}{\omega\left(\text{Im}\left(\frac{Z_s(T)}{\omega}\right)\right) + L_g)} \quad (2)$$

where σ_1 is the real part of the complex conductivity, σ_2 is the imaginary part of the complex conductivity, L_g is the geometrical inductance [50], μ_0 is the free space permeability, ω is the radian frequency, and $\delta_{\text{qp,theory}}$ is theoretical quasiparticle loss based on the CPW's complex conductivity. Therefore, by calculating the superconductive film's complex conductivity, we can find the contribution of quasiparticle loss

in superconductive CPW resonators. To evaluate the effect of resistive and inductive channels, we perform microwave spectroscopy measurements of our NbN resonators in the single-photon regime at sub-Kelvin temperature ranges and calculate superconducting film complex conductivity, which will be discussed in more detail in the next section.

A. CRYOGENIC MEASUREMENT OF MICROWAVE CPW RESONATORS

For microwave spectroscopy measurements, the CPW resonator chip was glued into a copper sample box and wire-bound with aluminum wire. The sample box was mounted inside an adiabatic demagnetization refrigerator (ADR). Note that the temperature sensor of the millikelvin stage was RuO_x, an effective and accurate low-temperature thermometer. In the ADR setup, complex microwave transmission spectroscopy (S_{21}) was conducted using an MS4642B Keysight vector network analyzer (VNA). To achieve the single-photon regime, the input power of the VNA (P_{VNA}) was set to -25 dBm. Subsequently, the VNA's input line was attenuated by -50 dB at room temperature. In addition, the VNA signal was attenuated by -20 dB at each stage of the ADR (at temperatures of 50, 4, and 0.8 K), resulting in a total attenuation (P_{att}) of -110 dB in the measurement setup. As this total attenuation was applied before the signals reached the sample's feed line, it effectively suppressed thermal noise, enabling the resonator to operate in the single-photon regime. Note that according to Fig. 3(a), which references the data from our previous measurement [22], the power range necessary to achieve the single-photon regime in the CPW feedline is between -134 and -136 dBm. This precisely matches the power level selected in this measurement setup. For all subsequent experiments, we consistently use an input power of $P_{\text{in}} = P_{\text{VNA}} + P_{\text{att}} = -135$ dBm. After the input signal went through the sample, an isolator was placed at the 4 K stage to prevent transmission signals from being contaminated by spurious reflections from the sample box. The signal was then amplified by a high electron mobility transistor at the 4 K stage, providing 40 dB amplification. In addition, a room temperature amplifier added an extra 45 dB amplification.

To investigate the temperature effects on propagation properties of NbN-based microwave CPWs, we measured full complex scattering data of our chips, as shown in Fig. 3(b), within the temperature ranges of 0.1 K $< T <$ 3 K. We observed noticeable Δf and amplitude reduction in $|S_{21}|$. We extracted CPW properties from $|S_{21}|$, such as Q_i and resonance frequency, (f_r), based on the notch-type resonator circuit model [51]. Extracted data confirm that at the single-photon regime, Q_i initially increases as the temperature rises since TLS defects are primarily responsible for losses in the $T < T_c/10$ regime [22]. With further temperature increase, TLS losses become negligible compared to quasiparticle losses, leading to a reduction in Q_i and a noticeable shift in f_r. Fig. 4(a) and (b) illustrates the relationship between Q_i and Δf in the 0.1 K $< T <$ 3 K ranges for both

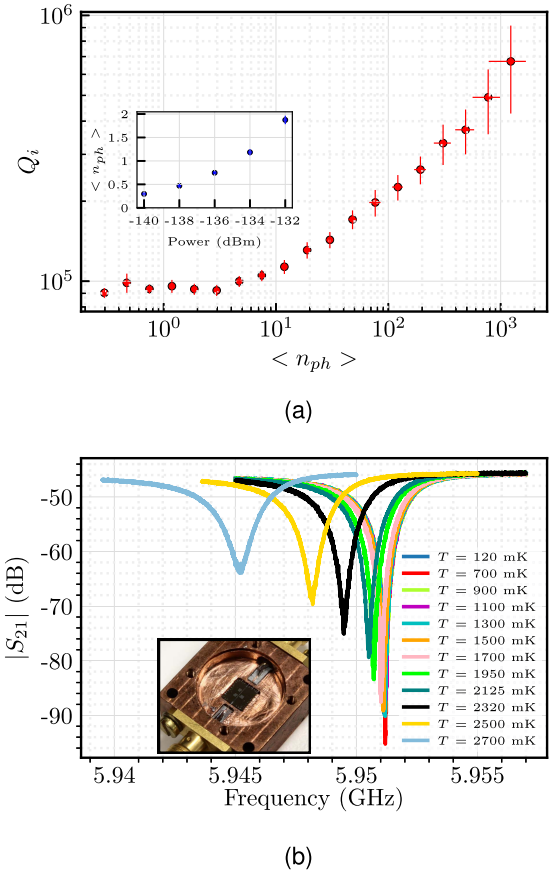

FIG. 3. (a) Q_i in the photon number ranges from $< n_{\text{ph}} > = 10^{-1}$ to 10^3 corresponding to the power ranges from $P_{\text{in}} = -140$ to -100 dBm at $T = 26$ mK, and $f_r = 5.95$ GHz, adapted from [22]. The inset plot shows the approximate $< n_{\text{ph}} >$ concerning input power inside the transmission line in the CPWs. In this plot, the input power to reach the single-photon regime is $P_{\text{in}} \simeq -135$ dBm. The vertical lines show Q_i uncertainty range, and the horizontal lines show $< n_{\text{ph}} >$ uncertainty range. The details about photon number calculation are illustrated in the appendix. (b) Microwave spectroscopy of NbN CPWs resonator at 0.1 K $< T <$ 3 K (in single-photon regime) at $P_{\text{in}} \simeq -135$ dBm. The inset shows the optical image of the NbN CPW chip being packaged for cryogenic microwave spectroscopy.

fundamental frequencies. In Fig. 4(a), Q_i increases from 10^5 at $T = 120$ mK to 2.571×10^5 at $T = 1$ K, and then decreases to 7.421×10^3 at $T = 2.9$ K at $f_r = 5.95$ GHz. Furthermore, Fig. 4(b) shows a red shift in the f_r starting between 1.6 and 1.8 K, which we speculate is due to an increase in the quasiparticle density in the inductive channel. To evaluate it, we calculate the complex conductivity of the NbN film in the next section.

B. COMPLEX CONDUCTIVITY CALCULATION OF CPW

As mentioned earlier, the propagation properties of the resonator, such as Q_i and f_r, depend on the CPW's impedance, which is extracted from the conductivity value of the superconductor film. Superconductor conductivity can be described by the two-fluid model (based on the Mattis–Bardeen theory [39]), where the real part of the conductivity describes the loss in the superconductor film, and the imaginary part exhibits the kinetic inductance value, leading to a resonance

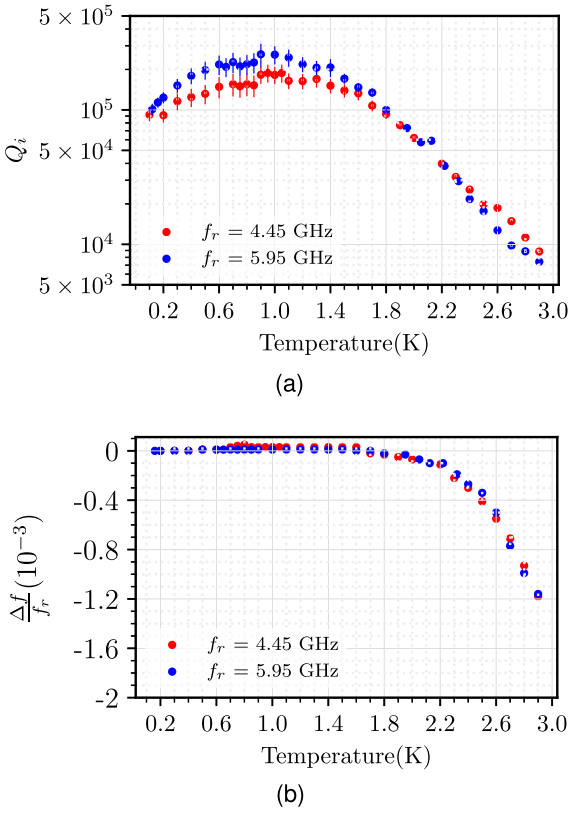

FIG. 4. (a) Q_i at single-photon regime versus temperature for f_r = 5.95 GHz and f_r = 4.45 GHz. (b) Δf at single-photon regime versus temperature for f_r = 5.95 GHz and f_r = 4.45 GHz.

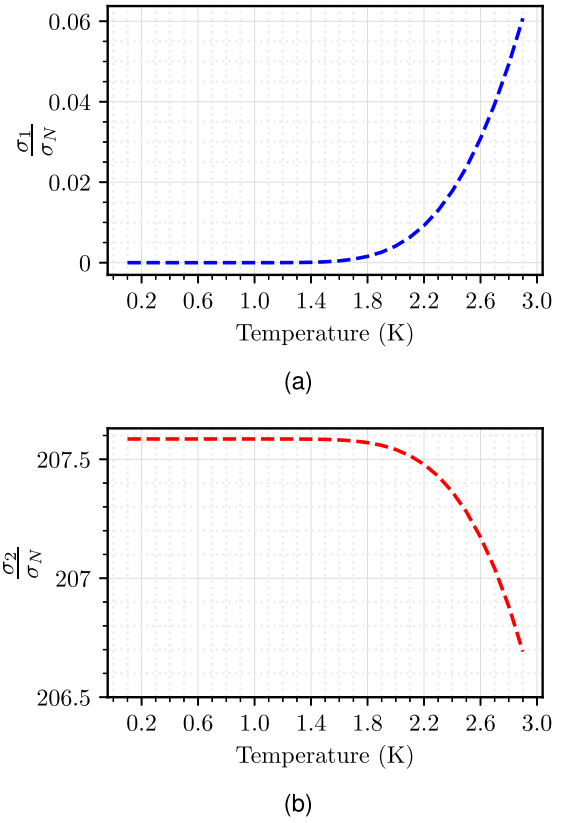

FIG. 5. (a) Real part of the normalized complex conductivity, σ_1, as a function of temperature. (b) Imaginary part of the normalized complex conductivity, σ_2, as a function of temperature for the NbN superconducting CPW resonator. Both plots are calculated at f_r = 5.95 GHz.

frequency shift. The superconductor's complex conductivity, $\sigma(T) = \sigma_1(T) - j\sigma_2(T)$, when $\hbar\omega \ll \Delta_0$ and $k_BT \ll \Delta_0$, is approximated as [48], [49]

$$\frac{\sigma_1(T)}{\sigma_N} = \frac{4\Delta_0}{\hbar\omega} e^{\left(-\frac{\Delta_0}{k_BT}\right)} \sinh\left(\frac{\hbar\omega}{2k_BT}\right) K_0\left(\frac{\hbar\omega}{2k_BT}\right) \quad (3)$$

$$\frac{\sigma_2(T)}{\sigma_N} = \frac{4\Delta_0}{\hbar\omega}\left[1 - \sqrt{\frac{2\pi k_BT}{\Delta_0}} \exp\frac{-\Delta_0}{k_BT} - 2\exp\frac{-\Delta_0}{k_BT} \exp\frac{-\hbar\omega}{2k_BT} I_0\left(\frac{\hbar\omega}{2k_BT}\right)\right] \quad (4)$$

where σ_N is normal state conductivity, $\Delta_0 = 1.76k_BT_c$ is the superconducting energy gap at zero temperature, k_B is Boltzmann's constant, $\hbar$ is the reduced plank constant, and $K_0(x)$ and $I_0(x)$ are modified Bessel functions of the second and first order, respectively.

The above equations allow us to calculate the NbN complex conductivity as a function of temperature. Fig. 5(a) and (b) illustrates σ_1 and σ_2 in the measured temperature range, respectively. Fig. 5(a) illustrates the relationship between increasing temperatures and NbN's resistive channel value, σ_1, which affects the quality factor of CPWs. Moreover, Fig. 5(b) describes an inductive channel, σ_2, of the NbN CPW, influencing the resonator frequency shift. This model is used to describe the complex conductivity of superconducting film and has provided information about the transition from TLS-dominated losses to quasiparticle losses [3]. However, Mattis–Bardeen theory assumes a thermal equilibrium quasiparticle distribution and does not account for nonequilibrium effects, such as quasiparticle trapping, diffusion, or photon-assisted generation, which can impact the response of high kinetic inductance materials, such as NbN.

Recent theoretical work has provided analytical descriptions of nonequilibrium quasiparticle distributions in superconducting resonators, revealing that photon-assisted quasiparticle heating and redistribution of quasiparticles can modify Q_i and f_r [52]. These effects become particularly relevant in NbN, where high kinetic inductance and increased photon absorption can increase nonequilibrium quasiparticle lifetimes, leading to deviations from conventional Mattis–Bardeen theory. A fully theoretical model comprising quasiparticle trapping, diffusion, and recombination effects of NbN would be an important future direction. However, the primary objective of this study is to experimentally characterize the quasiparticle density of NbN under varying temperatures, providing a foundation for future theoretical developments.

C. THERMAL AND NONEQUILIBRIUM QUASIPARTICLE DENSITY

To demonstrate the existence of nonequilibrium quasiparticle density, we need to compare the theoretical Q_i with the data

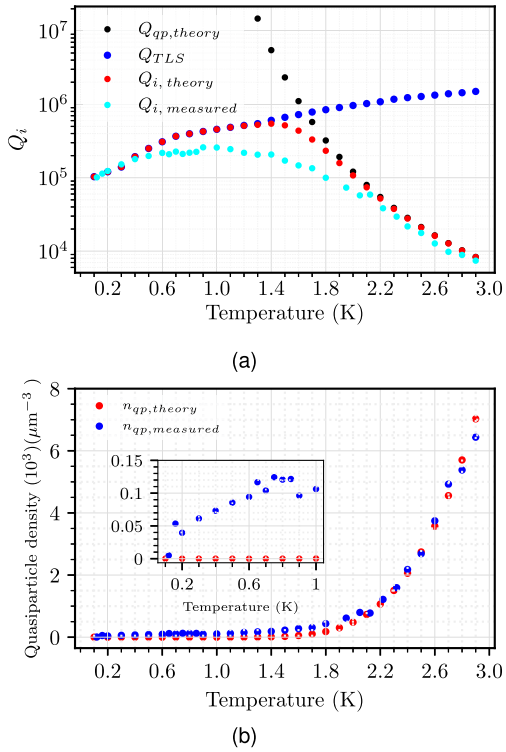

FIG. 6. (a) $Q_{i,\text{measured}}$ and $Q_{i,\text{theory}}$ versus temperature at $< n_{\text{ph}} > \sim 1$ fitted with the theoretical model of TLS and quasiparticle loss. Both plots are calculated and measured at $f_r = 5.95$ GHz. (b) Theoretical and measured quasiparticle density of NbN CPW. The inset shows quasiparticle density at $T < T_c/10$.

shown in Fig. 4(a). In this section and Fig. 6(a), we will differentiate between the measured and theoretically calculated internal quality factors, referring to them as $Q_{i,\text{measured}}$ and $Q_{i,\text{theory}}$, respectively. We will estimate $Q_{i,\text{theory}}$ within the temperature ranges between 0.1 K $< T <$ 3 K by calculating the TLS loss, Q_{TLS}, as evaluated in our previous study [22], as well as the thermal quasiparticle (2) with the below equation:

$$\frac{1}{Q_{i,\text{theory}}(T)} = \frac{1}{Q_{\text{TLS}}(T)} + \frac{1}{Q_{\text{qp,theory}}(T)} \tag{5}$$

where $Q_{\text{qp,Theroy}}(T)^{-1} = \delta_{\text{qp,Theory}}(T)$ is thermal quasiparticle loss coming from (2). Fig. 6(a) shows $Q_{\text{qp,Theory}}$, Q_{TLS}, and $Q_{i,\text{Theory}}(T)$ coming from (2), and $Q_{i,\text{measured}}$ adapting from Fig. 4(a). In Fig. 6(a), there is a deviation between the $Q_{i,\text{theory}}$ and $Q_{i,\text{measured}}$ in $T < T_c/10$. This deviation suggests the presence of another loss channel coming from nonequilibrium quasiparticle density.

To elaborate further, we calculated the nonequilibrium quasiparticle density in the CPWs in the next step. We used the following equations to determine the nonequilibrium quasiparticle density based on the measurement results [53]:

$$\delta_{\text{qp,measured}}(T) = \frac{1}{Q_{i,\text{measured}}(T)} - \frac{1}{Q_{\text{TLS}}(T)} \tag{6}$$

$$n_{\text{qp,measured}}(T) \sim \delta_{\text{qp,measured}}(T) N_0 \Delta(T) \frac{\pi}{\alpha} \sqrt{\frac{\hbar\omega}{2\Delta(T)}} \tag{7}$$

where $n_{\text{qp,measured}}(T)$ is quasiparticle density calculated from measurement results, $N_0 \sim 1.86 \times 10^{28}$ (state/m^{3}eV) is the density of states at the Fermi level from [47], [54], and α is the kinetic inductance ratio extracted from our previous study [22]. In addition, $\delta_{\text{qp,theory}}(T)$ in (2) can be utilized to extract quasiparticle density based on Mattis–Bardeen theory with the following equation:

$$n_{\text{qp,theory}}(T) \sim \delta_{\text{qp,theory}}(T) N_0 \Delta(T) \frac{\pi}{\alpha} \sqrt{\frac{\hbar\omega}{2\Delta(T)}} \tag{8}$$

Fig. 6(b) illustrates the theoretical and experimental quasiparticle density in 0.1 K $< T <$ 3 K. The inset in Fig. 6(b) experimentally confirms the presence of nonequilibrium quasiparticle density at temperatures much lower than T_c. In literature, quasiparticle density in the superconducting film at $T < T_c/10$ is negligible [55] because Cooper pair breaking and dissipating heat due to thermal quasiparticles rarely happen; however, we observed noticeable quasiparticle density at millikelvin temperature. In the inset of Fig. 6(b), quasiparticle density is saturating at 50 μm^{-3} at $T = 120$ mK, confirming a source of decoherence in quantum circuits at millikelvin temperature. We conclude that the noticeable saturation of quasiparticle density leads to a lower internal quality factor at low temperatures. As shown in Fig. 6(a), $Q_{i,\text{measured}}$ is lower than its predicted value. The same behavior has also been shown in other types of superconducting materials, such as Al and TiN superconducting CPWs [23], [56], [57]. However, NbN exhibits distinct nonequilibrium quasiparticle dynamics due to its shorter electron–phonon relaxation time ($\tau_{e-\text{ph}}$) and higher kinetic inductance compared to TiN and Al [3], [58], [59]. These properties make NbN particularly sensitive to quasiparticle-induced losses and impedance shifts, distinguishing it from conventional superconductors. Fig. 6(a) and (b) displays the noticeable nonequilibrium quasiparticle impact on superconducting film properties, particularly at millikelvin temperatures, where transmon qubits are measured. This study provides an experimental investigation into these effects, contributing to a deeper understanding of loss mechanisms in high kinetic inductance superconductors. Future works are needed to distinguish between intrinsic saturation and external nonequilibrium contributions.

Our microwave loss measurements provide evidence for quasiparticle saturation in superconducting films at millikelvin. However, to fully validate this phenomenon, complementary techniques, such as tunneling spectroscopy, are critical [52], [60]. These methods would allow for more direct measurements of quasiparticle dynamics, helping to distinguish between intrinsic quasiparticle effects and external perturbations coming from cryogenic setups and stray losses. In particular, understanding whether saturation is fundamentally driven by material properties or influenced by environmental factors, such as stray loss, is crucial for improving the performance of superconducting circuits.

In closing, we want to note that nonequilibrium quasiparticle density can be generated by the interaction between

electrons and phonons, resulting in the generation and recombination of quasiparticles. Indeed, microwave readout signals from VNA, essential for device operation, can generate nonequilibrium quasiparticles through photon absorption [5], [48], [53], [57], [61]. Note that our study could further extend to analyzing the quasiparticle density in NbN films fabricated via atomic layer deposition.

V. CONCLUSION

In this study, we performed detailed temperature-dependent cryogenic microwave spectroscopy of NbN CPW operating in the single-photon regime. Our results demonstrate that both TLS and quasiparticle defects contribute to performance degradation in NbN superconducting resonators. In addition, we calculated the complex conductivity of NbN films, capturing the dissipative and dispersive effects on the CPW due to quasiparticle defects. We then presented Q_i and f_r in response to temperature changes. Subsequently, we verified the effect of thermal and nonequilibrium quasiparticle density on Q_i. Our results show that a noticeable nonequilibrium quasiparticle density exists at millikelvin temperatures, leading to decoherence in quantum circuits. These findings deepen understanding of quasiparticle-induced losses and support the development of robust superconducting quantum circuits.

APPENDIX
PHOTON NUMBER CALCULATION

We can derive the photon number inside the resonator with the following equations [62]:

$$P_{\text{in}} = P_{\text{trans}} + P_{\text{reflection}} + P_{\text{loss}} \tag{9}$$

$$P_{\text{loss}} = P_{\text{in}}(1 - |S_{21}|^2 - |S_{11}|^2) \tag{10}$$

$$|S_{21}| = |Q_c|^{-2}(|Q_c|^2 + Q_l^2 - 2Q_l|Q_c|) \tag{11}$$

$$|S_{11}| = Q_l^2/|Q_c|^2 \tag{12}$$

$$< n_{\text{ph}} >= Q_i \times \frac{P_{\text{loss}}}{\hbar\omega^2} \tag{13}$$

where $< n_{\text{ph}} >$ is the photon number, $P_{\text{in}} = P_{\text{VNA}} + P_{\text{att}}$ is the input power inside the chip, P_{trans} is the transmitted power through the feedline, P_{loss} is the source of losses in the chip, Q_l is loaded quality factor, and Q_c is coupling quality factor.

ACKNOWLEDGMENT

This study made use of the University of Glasgow James Watt Nanofabrication Centre (JWNC), and the authors would like to thank JWNC technical staff for their support.

REFERENCES

[1] I. Siddiqi, "Engineering high-coherence superconducting qubits," *Nature Rev. Mater.*, vol. 6, no. 10, pp. 875–891, 2021, doi: 10.1038/s41578-021-00370-4.

[2] J. Aumentado, M. W. Keller, J. M. Martinis, and M. H. Devoret, "Nonequilibrium quasiparticles and 2*e* periodicity in single-Cooper-pair transistors," *Phys. Rev. Lett.*, vol. 92, no. 6, 2004, Art. no. 066802, doi: 10.1103/PhysRevLett.92.066802.

[3] J. Zmuidzinas, "Superconducting microresonators: Physics and applications," *Annu. Rev. Condens. Matter Phys.*, vol. 3, no. 1, pp. 169–214, 2012, doi: 10.1146/annurev-conmatphys-020911-125022.

[4] P. K. Day, H. G. LeDuc, B. A. Mazin, A. Vayonakis, and J. Zmuidzinas, "A broadband superconducting detector suitable for use in large arrays," *Nature*, vol. 425, no. 6960, pp. 817–821, 2003, doi: 10.1038/nature02037.

[5] D. V. Morozov, A. Casaburi, and R. H. Hadfield, "Superconducting photon detectors," *Contemporary Phys.*, vol. 62, no. 2, pp. 69–91, 2021, doi: 10.1080/00107514.2022.2043596.

[6] M. Lenander et al., "Measurement of energy decay in superconducting qubits from nonequilibrium quasiparticles," *Phys. Rev. B*, vol. 84, no. 2, Art. no. 024501, doi: 10.1103/PhysRevB.84.024501.

[7] J. Aumentado, G. Catelani, and K. Serniak, "Quasiparticle poisoning in superconducting quantum computers," *Phys. Today*, vol. 76, no. 8, pp. 34–39, 2023, doi: 10.1063/PT.3.5291.

[8] J. Burnett, A. Bengtsson, D. Niepce, and J. Bylander, "Noise and loss of superconducting aluminium resonators at single photon energies," in *Proc. J. Phys.: Conf. Ser.*, vol. 969, no. 1, 2018, Art. no. 012131, doi: 10.1088/1742-6596/969/1/012131.

[9] D. S. Wisbey et al., "Effect of metal/substrate interfaces on radio-frequency loss in superconducting coplanar waveguides," *J. Appl. Phys.*, vol. 108, no. 9, 2010, Art. no. 093918, doi: 10.1063/1.3499608.

[10] D. Pitsun et al., "Cross coupling of a solid-state qubit to an input signal due to multiplexed dispersive readout," *Phys. Rev. Appl.*, vol. 14, no. 5, 2020, Art. no. 054059, doi: 10.1103/PhysRevApplied.14.054059.

[11] C. Wang et al., "Measurement and control of quasiparticle dynamics in a superconducting qubit," *Nature Commun.*, vol. 5, no. 1, 2014, Art. no. 5836, doi: 10.1038/ncomms6836.

[12] C. D. Wilen et al., "Correlated charge noise and relaxation errors in superconducting qubits," *Nature*, vol. 594, no. 7863, pp. 369–373, 2021, doi: 10.1038/s41586-021-03557-5.

[13] G. Catelani and J. P. Pekola, "Using materials for quasiparticle engineering," *Mater. Quantum Technol.*, vol. 2, no. 1, 2022, Art. no. 013001, doi: 10.1088/2633-4356/ac4a75.

[14] X. Pan et al., "Engineering superconducting qubits to reduce quasiparticles and charge noise," *Nature Commun.*, vol. 13, no. 1, 2022, Art. no. 7196, doi: 10.1038/s41467-022-34727-2.

[15] R.-P. Riwar and G. Catelani, "Efficient quasiparticle traps with low dissipation through gap engineering," *Phys. Rev. B*, vol. 100, no. 14, 2019, Art. no. 144514, doi: 10.1103/PhysRevB.100.144514.

[16] P. Kamenov, T. DiNapoli, M. Gershenson, and S. Chakram, "Suppression of quasiparticle poisoning in transmon qubits by gap engineering," 2023, *arXiv:2309.02655*, doi: 10.48550/arXiv.2309.02655.

[17] F. Henriques et al., "Phonon traps reduce the quasiparticle density in superconducting circuits," *Appl. Phys. Lett.*, vol. 115, no. 21, 2019, Art. no. 212601, doi: 10.1063/1.5124967.

[18] T. Connolly et al., "Coexistence of nonequilibrium density and equilibrium energy distribution of quasiparticles in a superconducting qubit," *Phys. Rev. Lett.*, vol. 132, 2024, Art. no. 217001, doi: 10.1103/PhysRevLett.132.217001.

[19] S. Gustavsson et al., "Suppressing relaxation in superconducting qubits by quasiparticle pumping," *Science*, vol. 354, no. 6319, pp. 1573–1577, 2016, doi: 10.1126/science.aah5844.

[20] R. Aguado, "A perspective on semiconductor-based superconducting qubits," *Appl. Phys. Lett.*, vol. 117, no. 24, 2020, Art. no. 240501, doi: 10.1063/5.0024124.

[21] E. Prada et al., "From Andreev to Majorana bound states in hybrid superconductor–semiconductor nanowires," *Nature Rev. Phys.*, vol. 2, no. 10, pp. 575–594, 2020, doi: 10.1038/s42254-020-0228-y.

[22] P. Foshat et al., "Characterizing niobium nitride-based superconducting coplanar waveguide resonators for microwave hybrid circuit quantum electrodynamics," *IEEE Trans. Appl. Supercond.*, vol. 35, no. 3, May 2025, Art. no. 0601116, doi: 10.1109/TASC.2025.3532821.

[23] A. Alexander, C. G. Weddle, and C. J. Richardson, "Power and temperature dependent model for high Q superconductors," *APL Quantum*, vol. 2, 2025, Art. no. 036102, doi: doi: 10.1063/5.0273506.

[24] D. P. Pappas, M. R. Vissers, D. S. Wisbey, J. S. Kline, and J. Gao, "Two level system loss in superconducting microwave resonators," *IEEE Trans. Appl. Supercond.*, vol. 21, no. 3, pp. 871–874, Jun. 2011, doi: 10.1109/TASC.2010.2097578.

[25] L. Grünhaupt et al., "Loss mechanisms and quasiparticle dynamics in superconducting microwave resonators made of thin-film granular aluminum," *Phys. Rev. Lett.*, vol. 121, no. 11, 2018, Art. no. 117001, doi: 10.1103/PhysRevLett.121.117001.

[26] T. Noguchi, S. Mima, and C. Otani, "Contribution of residual quasiparticles to the characteristics of superconducting thin-film resonators," *IEEE Trans. Appl. Supercond.*, vol. 31, no. 5, Aug. 2021, Art. no. 2400205, doi: 10.1109/TASC.2021.3058075.

[27] R. Barends et al., "Niobium and tantalum high Q resonators for photon detectors," *IEEE Trans. Appl. Supercond.*, vol. 17, no. 2, pp. 263–266, Jun. 2007, doi: 10.1109/TASC.2007.898541.

[28] C. Song, "Microwave properties of vortices in superconducting resonators," Ph.D. dissertation, Syracuse Univ., Syracuse, NY, USA, 2011. [Online]. Available: https://surface.syr.edu/cgi/viewcontent.cgi?article=1118&context=phy_etd

[29] M. Müller et al., "Magnetic field robust high quality factor NbTiN superconducting microwave resonators," *Mater. Quantum Technol.*, vol. 2, no. 1, 2022, Art. no. 015002, doi: 10.1088/2633-4356/ac50f8.

[30] J. M. Sage, V. Bolkhovsky, W. D. Oliver, B. Turek, and P. B. Welander, "Study of loss in superconducting coplanar waveguide resonators," *J. Appl. Phys.*, vol. 109, no. 6, 2011, Art. no.063915, doi: 10.1063/1.3552890.

[31] S. Hähnle et al., "Suppression of radiation loss in high kinetic inductance superconducting co-planar waveguides," *Appl. Phys. Lett.*, vol. 116, no. 18, 2020, Art. no. 182601, doi: 10.1063/5.0005047.

[32] P. De Visser, J. Baselmans, S. Yates, P. Diener, A. Endo, and T. Klapwijk, "Microwave-induced excess quasiparticles in superconducting resonators measured through correlated conductivity fluctuations," *Appl. Phys. Lett.*, vol. 100, no. 16, 2012, Art. no. 162601, doi: 10.1063/1.4704151.

[33] S. A. De Rooij, J. J. Baselmans, V. Murugesan, D. J. Thoen, and P. J. De Visser, "Strong reduction of quasiparticle fluctuations in a superconductor due to decoupling of the quasiparticle number and lifetime," *Phys. Rev. B*, vol. 104, no. 18, 2021, Art. no. L180506, doi: 10.1103/PhysRevB.104.L180506.

[34] J. Hu et al., "Investigation of quasi-particle relaxation in strongly disordered superconductor resonators," *Supercond. Sci. Technol.*, vol. 37, no. 5, 2024, Art. no. 055014, doi: 10.1088/1361-6668/ad3f80.

[35] L. Zhang, L. You, W. Peng, and Z. Wang, "Quasiparticle scattering time in NbN superconducting thin films," *Physica C: Supercond. Appl.*, vol. 579, 2020, Art. no. 1353773, doi: 10.1016/j.physc.2020.1353773.

[36] M. Drimmer et al., "The effect of niobium thin film structure on losses in superconducting circuits," 2024, *arXiv:2403.12164*, doi: 10.48550/arXiv.2403.12164.

[37] S. Poorgholam-Khanjari et al., "Engineering high-Q superconducting tantalum microwave coplanar waveguide resonators for compact coherent quantum circuits," *Sci. Rep.*, vol. 15, 2025, Art. no. 27113, doi: 10.1038/s41598-025-11744-x.

[38] R. Barends, "Photon-detecting superconducting resonators," Ph.D. thesis, Tech. Univ. Delft, Delft, The Netherlands, 2009. [Online]. Available: https://resolver.tudelft.nl/uuid:574944e6-c3ce-4c86-a511-a88385b22379

[39] D. C. Mattis and J. Bardeen, "Theory of the anomalous skin effect in normal and superconducting metals," *Phys. Rev.*, vol. 111, no. 2, 1958, Art. no. 412, doi: 10.1103/PhysRev.111.412.

[40] A. Banerjee et al., "Optical properties of refractory metal based thin films," *Opt. Mater. Exp.*, vol. 8, no. 8, pp. 2072–2088, 2018, doi: 10.1364/OME.8.002072.

[41] M. J. Sowa et al., "Plasma-enhanced atomic layer deposition of superconducting niobium nitride," *J. Vac. Sci. Technol. A*, vol. 35, no. 1, 2017, Art. no. 01B143, doi: 10.1116/1.4972858.

[42] E. Knehr et al., "Wafer-level uniformity of atomic-layer-deposited niobium nitride thin films for quantum devices," *J. Vac. Sci. Technol. A*, vol. 39, no. 5, 2021, Art. no. 052401, doi: 10.1116/6.0001126.

[43] H. Shi et al., "NBN films on flexible and thickness controllable dielectric substrates," *Sci. Rep.*, vol. 12, no. 1, 2022, Art. no. 10662, doi: 10.1038/s41598-022-14861-z.

[44] C. Lennon et al., "High-uniformity atomic layer deposition of superconducting niobium nitride thin films for quantum photonic integration," *Mater. Quantum Technol.*, vol. 3, no. 4, 2023, Art. no. 045401, doi: 10.1088/2633-4356/ad0aa5.

[45] J. Alfonso, J. Buitrago, J. Torres, J. Marco, and B. Santos, "Influence of fabrication parameters on crystallization, microstructure, and surface composition of NbN thin films deposited by RF magnetron sputtering," *J. Mater. Sci.*, vol. 45, pp. 5528–5533, 2010, doi: 10.1007/s10853-010-4612-3.

[46] Q. Zhang, H. Wang, X. Tang, W. Peng, and Z. Wang, "Superconductivity dependence on epitaxial NBN film thickness," *IEEE Trans. Appl. Supercond.*, vol. 29, no. 5, Aug. 2019, Art. no. 7500305, doi: 10.1109/TASC.2019.2902032.

[47] D. Hazra et al., "Superconducting properties of very high quality NbN thin films grown by high temperature chemical vapor deposition," *Supercond. Sci. Technol.*, vol. 29, no. 10, 2016, Art. no. 105011, doi: 10.1088/0953-2048/29/10/105011.

[48] A. Alexander, "Measuring and trapping quasiparticles in superconducting coplanar waveguide resonators," Ph.D. dissertation, Univ. Maryland, College Park, MD, USA, 2021, doi: 10.13016/0t9f-xqfe.

[49] J. Gao, "The physics of superconducting microwave resonators," Ph.D. dissertation, California Inst. Technol., Pasadena, CA, USA, 2008. [Online]. Available: http://www.submm.caltech.edu/~jonas/Theses/Jiansong_Gao_08.pdf

[50] M. Göppl et al., "Coplanar waveguide resonators for circuit quantum electrodynamics," *J. Appl. Phys.*, vol. 104, no. 11, 2008, Art. no. 113904, doi: 10.1063/1.3010859.

[51] S. Probst, F. Song, P. A. Bushev, A. V. Ustinov, and M. Weides, "Efficient and robust analysis of complex scattering data under noise in microwave resonators," *Rev. Sci. Instrum.*, vol. 86, no. 2, 2015, Art. no. 024706, doi: 10.1063/1.4907935.

[52] P. Fischer and G. Catelani, "Nonequilibrium quasiparticle distribution in superconducting resonators: An analytical approach," *Phys. Rev. Appl.*, vol. 19, no. 5, 2023, Art. no. 054087, doi: 10.1103/PhysRevApplied.19.054087.

[53] R. Barends et al., "Minimizing quasiparticle generation from stray infrared light in superconducting quantum circuits," *Appl. Phys. Lett.*, vol. 99, no. 11, 2011, Art. no. 113507, doi: 10.1063/1.3638063.

[54] S. Chockalingam, M. Chand, J. Jesudasan, V. Tripathi, and P. Raychaudhuri, "Superconducting properties and hall effect of epitaxial nbn thin films," *Phys. Rev. B*, vol. 77, no. 21, 2008, Art. no. 214503, doi: 10.1103/PhysRevB.77.214503.

[55] C. Wilson and D. Prober, "Quasiparticle number fluctuations in superconductors," *Phys. Rev. B*, vol. 69, no. 9, 2004, Art. no. 094524, doi: 10.1103/PhysRevB.69.094524.

[56] R. Budoyo et al., "Effects of nonequilibrium quasiparticles in a thin-film superconducting microwave resonator under optical illumination," *Phys. Rev. B*, vol. 93, no. 2, 2016, Art. no. 024514, doi: 10.1103/PhysRevB.93.024514.

[57] P. De Visser, J. Baselmans, P. Diener, S. Yates, A. Endo, and T. Klapwijk, "Number fluctuations of sparse quasiparticles in a superconductor," *Phys. Rev. Lett.*, vol. 106, no. 16, 2011, Art. no. 167004, doi: 10.1103/PhysRevLett.106.167004.

[58] D. Ristè, C. Bultink, M. J. Tiggelman, R. N. Schouten, K. W. Lehnert, and L. DiCarlo, "Millisecond charge-parity fluctuations and induced decoherence in a superconducting transmon qubit," *Nature Commun.*, vol. 4, no. 1, 2013, Art. no. 1913, doi: 10.1038/ncomms2936.

[59] T. Guruswamy, D. Goldie, and S. Withington, "Quasiparticle generation efficiency in superconducting thin films," *Superconductor Sci. Technol.*, vol. 27, no. 5, 2014, Art. no. 055012, doi: 10.1088/0953-2048/27/5/055012.

[60] K. R. Joshi et al., "Quasiparticle spectroscopy, transport, and magnetic properties of Nb films used in superconducting qubits," *Phys. Rev. Appl.*, vol. 20, no. 2, 2023, Art. no. 024031, doi: 10.1103/PhysRevApplied.20.024031.

[61] P. De Visser, D. Goldie, P. Diener, S. Withington, J. Baselmans, and T. Klapwijk, "Evidence of a nonequilibrium distribution of quasiparticles in the microwave response of a superconducting aluminum resonator," *Phys. Rev. Lett.*, vol. 112, no. 4, 2014, Art. no. 047004, doi: 10.1103/PhysRevLett.112.047004.

[62] A. Bruno, G. De Lange, S. Asaad, K. Van Der Enden, N. Langford, and L. DiCarlo, "Reducing intrinsic loss in superconducting resonators by surface treatment and deep etching of silicon substrates," *Appl. Phys. Lett.*, vol. 106, no. 18, 2015, Art. no. 182601, doi: 10.1063/1.4919761.